Exchange-Torque-Triggered Fast Switching of Antiferromagnetic Domains

Jia Xu[ORCID],[1,3,*] Jing Xia,[2,7,*] Xichao Zhang[ORCID],[8,*] Chao Zhou[ORCID],[1,3] Dong Shi,[1] Haoran Chen,[1] Tong Wu,[1] Qian Li,[4] Haifeng Ding[ORCID],[5] Yan Zhou,[2,†] and Yizheng Wu[ORCID][1,6,‡]

[1]*Department of Physics and State Key Laboratory of Surface Physics, Fudan University, Shanghai 200433, China*
[2]*School of Science and Engineering, The Chinese University of Hong Kong, Shenzhen, Guangdong 518172, China*
[3]*Institute of Physics, Shaanxi University of Technology, Hanzhong 723001, China*
[4]*National Synchrotron Radiation Laboratory, University of Science and Technology of China, Hefei 230029, China*
[5]*National Laboratory of Solid State Microstructures, Department of Physics, Nanjing University, Nanjing 210093, China*
[6]*Shanghai Research Center for Quantum Sciences, Shanghai 201315, China*
[7]*College of Physics and Electronic Engineering, Sichuan Normal University, Chengdu 610068, China*
[8]*Department of Electrical and Computer Engineering, Shinshu University, 4-17-1 Wakasato, Nagano 380-8553, Japan*

The antiferromagnet is considered to be a promising hosting material for the next generation of magnetic storage due to its high stability and stray-field-free property. Understanding the switching properties of the antiferromagnetic (AFM) domain state is critical for developing AFM spintronics. By utilizing the magneto-optical birefringence effect, we experimentally demonstrate the switching rate of the AFM domain can be enhanced by more than 2 orders of magnitude through applying an alternating square-wave field on a single crystalline Fe/CoO bilayer. The observed extraordinary speed can be much faster than that triggered by a constant field with the same amplitude. The effect can be understood as the efficient suppression of the pinning of AFM domain walls by the strong exchange torque triggered by the reversal of the Fe magnetization, as revealed by spin dynamics simulations. Our finding opens up new opportunities to design the antiferromagnet-based spintronic devices utilizing the ferromagnet-antiferromagnet heterostructure.

Recent experimental demonstrations of electrical switching and detection of antiferromagnetic (AFM) spins have opened up a new route toward information storage devices based on antiferromagnets [1–12]. In comparison with its counterpart, ferromagnet, the antiparallel spin among sublattices in antiferromagnets produce zero dipolar fields, making them inert to the external field perturbations [1–4,13–15], and also allowing multilevel stability in memory devices [16,17]. The information storage in AFM memory relies on the effective manipulation of the Néel vector orientation, thus it becomes critically important to understand the switching dynamics of AFM domains, which is still poorly explored due to the great challenge to detect the AFM spin states at the microscopic scale [18]. Although the photoemission electron microscopy based on the x-ray magnetic linear dichroism (XMLD) effect [19] provides an effective way to detect the AFM domains with high resolution, and was also applied to image the change of AFM domain states after being excited by current or field pulses, it is still difficult to study the real-time evolution of AFM domains under the electrical current or magnetic field. AFM domain imaging with high resolution can also be achieved through the techniques based on the scanning methods [20–24], which are hard to study the time-dependent AFM domain switching process. Such difficulty of real-time imaging of the AFM domains

may be overcome by the magneto-optical birefringence (MOB) effect, which has been demonstrated to optically image the AFM domain in NiO and CoO films [25,26] and AFM domain switching in NiO/Pt bilayers by current pulses [27].

The electronical readout of the Néel vector orientation in an antiferromagnet spintronic device also poses another challenge. Although the switching of AFM spins can be electrically detected by the anisotropic magnetoresistance (MR) [1–4], the spin Hall MR [5–8,13], and the related planar Hall resistance [14,15], the associated MR is usually too small for the applications [28–30]. In the ferromagnet-antiferromagnet heterostructure, by taking advantage of the larger MR in the ferromagnet, e.g., based on tunneling MR of ferromagnet-MgO-ferromagnet junctions, the strong coupling between the ferromagnetic (FM) and AFM spins may provide an alternative solution to effectively read out the information stored in the AFM spins [31,32]. In such ferromagnet-antiferromagnet spintronic devices, the key is how to effectively write the information into the AFM spins, which still relies on the understanding and manipulation of dynamical switching process of AFM domains. However, most previous studies on the ferromagnet-antiferromagnet systems were based on the exchange bias effect with the goal to stabilize the FM spin orientation by AFM spins. The XMLD measurements demonstrated the

exchange coupling can manipulate the interfacial Néel vector through an exchange spring mechanism [32], but the understanding on the dynamical switching process of AFM domains is still missing.

In this Letter, we demonstrate the dynamic switching of CoO AFM domains in a single-crystalline Fe/CoO(001) bilayer under an external magnetic field by the MOB effect. We find a significant acceleration of the switching speed through a square-wave alternating (ac) magnetic field with more than 2 orders of magnitude faster than that induced by a constant (dc) field with the same amplitude. Spin dynamics simulations prove that the ac field driven ferromagnet magnetization reversal can induce a strong exchange torque inside the AFM domain wall (DW), resulting a strong acceleration of AFM domain switching. Effective manipulation of AFM domain switching by the ac field not only deepens the understanding on the AFM spin dynamics, but also opens up new opportunities to design functional spintronic devices based on the ferromagnet-antiferromagnet bilayer structures. CoO has the G-type AFM spin structure with a spin-compensated (001) surface. In an Fe/CoO(001) system, the Fe spins $\vec{s}_{Fe}$ and the CoO AFM spins $\overleftrightarrow{s}_{CoO}$ are coupled orthogonally by the spin-flop coupling [33,34]. Thus, $\overleftrightarrow{s}_{CoO}$ is possible to be manipulated by $\vec{s}_{Fe}$ through the interfacial exchange coupling [33,35,36]. In order to study the dynamic switching behavior of the CoO domain in real time, we prepared a single crystal MgO(4 nm)/Fe(5 nm)/ CoO(5 nm) sample grown on a MgO(001) substrate [33,35,37]. The Néel vectors of CoO/MgO(001) have been determined along either [110] or [1$\bar{1}$0] directions in different AFM domains [33]. If the field cooling is performed with the cooling field H_{FC} along [110], the interfacial spin-flop coupling aligns $\overleftrightarrow{s}_{CoO}$ perpendicular to H_{FC}, and only uniform contrast can be observed. At an elevated temperature, it is expected that, by applying a magnetic field perpendicular to H_{FC}, the antiferromagnet domains will gradually form with the AFM spins switched by 90° due to strong interfacial exchange coupling and thermal activation [33,35,37]. Such a concept of the AFM domain switching process shown in Figs. 1(a)–1(d), however, has not been directly confirmed in real space due to the difficulty of imaging the AFM domain under a magnetic field.

The AFM CoO domain during the switching process can be directly imaged with the MOB effect [26]. The sample was first cooled from 330 K down to 77 K with H_{FC} = 1000 Oe along CoO[1$\bar{1}$0]. Figure 1(e) shows the birefringence image measured at zero field after the field cooling using a commercial Kerr microscope equipped with a blue LED source, and the observed uniform contrast indicates a single AFM domain state in CoO film. Then, we applied a dc field of 900 Oe along CoO[110] at 232 K, and kept measuring the birefringence images with an interval of one second. Figures 1(f)–1(h) show the AFM domain images at different times after applying the field, which clearly
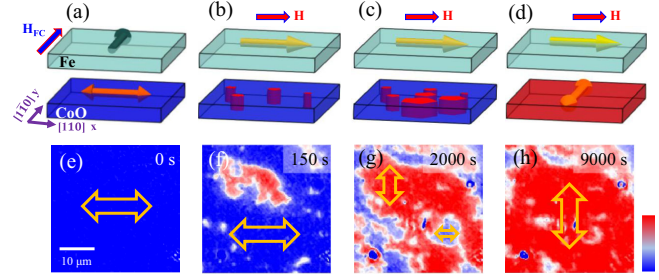
FIG. 1. (a)–(d) Schematic illustration of the evolution of spin configurations in Fe/CoO bilayer after the field cooling with H_{FC} and under a constant field with $H{\perp}H_{FC}$. (e),(f) Corresponding AFM domains measured with H = 900 Oe at 232 K.

demonstrate the gradual evolution of AFM domains. Since $\overleftrightarrow{s}_{CoO}$ is perpendicular to $\vec{s}_{Fe}$ [40], the blue and red contrasts in Fig. 1 correspond to $\overleftrightarrow{s}_{CoO}\|\langle110\rangle$ and $\overleftrightarrow{s}_{CoO}\|\langle1\bar{1}0\rangle$, respectively. Thus, our results prove that the time-dependent AFM spin orientation evolution under a constant field can be directly imaged by the MOB effect. Since the MOB signal from a 5-nm-thick Fe film is negligibly small, the observed contrast in the Fe/CoO bilayer mainly comes from the CoO layer [32,37].

The AFM domain switching process in Fe/CoO(001) has been investigated indirectly through the measurement of the remanent Kerr signal by alternately switching the Fe magnetization [33,35]. Since AFM domains can be imaged through the MOB effect within strong magnetic fields, it's possible to identify the effect of Fe magnetization reversal by monitoring the CoO domain distribution in real time. We first cooled down the sample with $H_{FC}\|[1\bar{1}0]$, then imaged the CoO domain distributions while applying an ac field of 900 Oe along $\langle110\rangle$ with a duration time $\Delta t = 1$ s [Fig. 2(a)]. Figures 2(b)–2(e) show the representative CoO domains at different times. The CoO domains change from blue into red, indicating the switching of $\overleftrightarrow{s}_{CoO}$ from $\langle110\rangle$ to $\langle1\bar{1}0\rangle$. We found that the domain switching was almost completed at the time of 30 s, which is in sharp contrast to the switching time longer than 9000 s induced by a dc field in Fig. 1. Therefore, the dynamic switching of AFM domains driven by ac fields is much faster than that triggered by dc fields.

In order to understand the effect of the magnetic field on the evolution of AFM domains, we quantitatively analyzed the area S of the switched CoO domains at different times. Figure 2(f) clearly shows that under the ac field, the AFM domain switching occurs faster by 2 orders of magnitude than that driven by the dc field. Moreover, the observed time-dependent switching is almost identical for the dc field along either [$\bar{1}\bar{1}0$] or [110], in good agreement with the 90° switching behavior of AFM domains.

In general, the AFM domain switching process includes the domain nucleation and growth processes, and becomes faster at higher temperatures due to thermal activation.
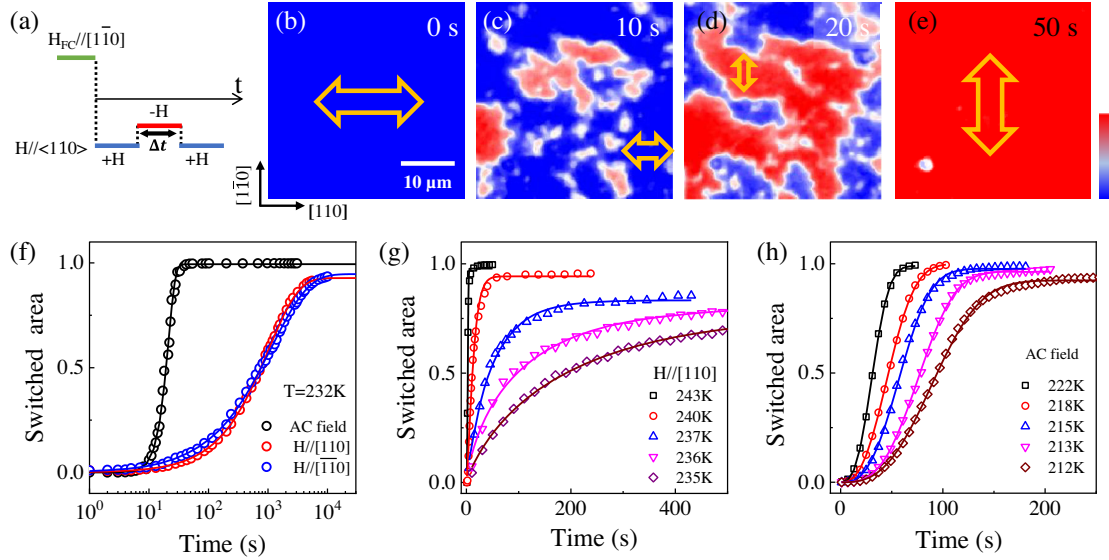
FIG. 2. (a) Schematic of the ac field in the measurement. (b)–(e) Time-dependent AFM domain evolution under $H_{ac} = 900$ Oe at 232 K with $\Delta t = 1$ s. (f) Time-dependent switched area S of AFM domain under dc fields or ac fields, the solid lines represent the fitted results using Eq. (1). (g),(h) Time dependence of S at different temperatures under dc or ac fields with $\Delta t = 3$ s. Amplitudes of both dc and ac fields are 900 Oe.

Figure 2(g) shows that the switched area increases quickly right after applying the dc field, and then gradually slows down until saturation, which is similar to the training effect [47,48]. The switching time reduces by more than one order of magnitude for the temperatures from 243 to 235 K, demonstrating the essential role of thermal activation on the AFM domain switching.

The temperature-dependent effect on CoO AFM domain switching was also investigated under the ac field, as shown in Fig. 2(h). The ac field was applied with $H_{ac} = 900$ Oe and $\Delta t = 3$ s in a lower temperature range between 212 and 222 K. S increases slowly at the beginning, gets faster in the middle, and then slows down again to approach to the

saturation, which can be attributed to the competition between domain nucleation and domain growth mechanisms [33,35]. We also investigated the time-dependent S at 215 K under an ac field with $H_{ac} = 900$ Oe and different Δt. Figure 3(a) shows that the domain switching process is faster for the shorter Δt. The inset shows an expanded local region of the measured curve with $\Delta t = 7$ s. It apparently shows that the domain switching mainly happens right after reversing the field direction, and the domain area during Δt remains constant. Figures 3(b)–3(d) show the representative domain images before and after field switching at the time t_0, t_1, and t_2, as marked in Fig. 3(a). The differential image between t_0 and t_1 in Fig. 3(e) demonstrates the
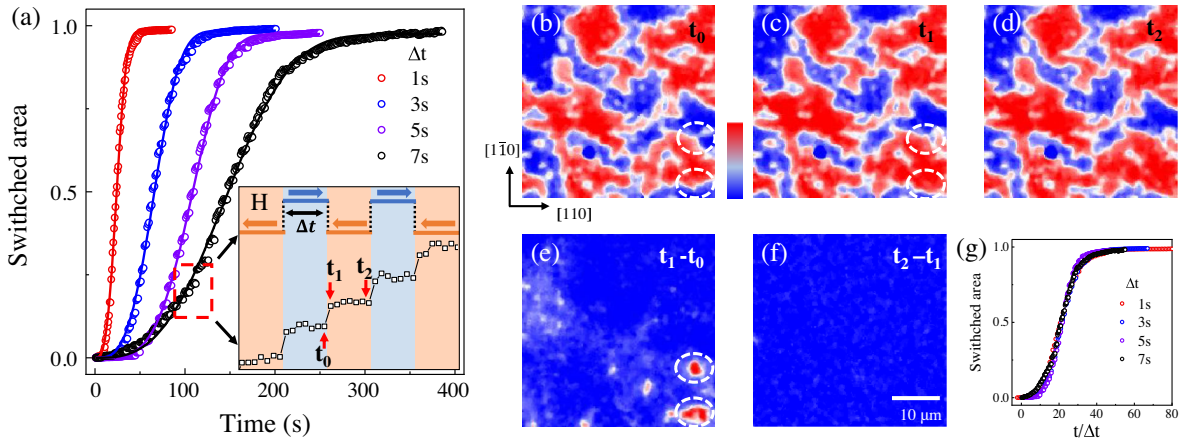
FIG. 3. (a) Time dependence of S with different Δt under $H_{ac} = \pm 900$ Oe at 215 K. The solid lines are fitting curves using Eq. (1). The inset is an enlarged view of the red dash area. (b)–(d) AFM domain image at the time of t_0, t_1, and t_2 as marked by the arrows in (a). (e) Differential image between (b) and (c). (f) Differential image between (c) and (d). (g) S as a function of normalized $t/\Delta t$.

domain growth by field switching, as indicated by the white circles. The differential image between t_1 and t_2 in Fig. 3(f) shows zero difference during the duration time. Besides, if we normalize the time with Δt, all the curves in Fig. 3(a) fall into one curve, as shown in Fig. 3(g).

To reveal the mechanism behind the process, we quantitatively analyzed the experimental data. It is known that the switching of AFM domains can be described by the Kolmogorov-Avrami model, which contains an extended exponential formula [33,35,47,49]:

$$S = 1 - \exp[-(t/\tau_D)^\sigma]. \tag{1}$$

Here, t is time, σ is a power index, and τ_D is the relaxation time constant. The time-dependent S shown in Figs. 2(f)–2(h) can be well fitted by Eq. (1), indicating that the Kolmogorov-Avrami model is valid in describing the switching process.

The energy barrier E_b of AFM domain switching can be quantified through temperature-dependent τ_D based on the Arrhenius law [37,42]. The fitted E_b is (2.70 ± 0.70) eV under the dc field of 900 Oe, and (0.44 ± 0.03) eV under the ac field. The lower energy barrier under ac fields makes the domain switching much faster.

In the following, we propose a model to explain the microscopic origin of the enhanced AFM domain growth rate by the field reversing. In Fe/CoO(001), $\overleftrightarrow{s}_{CoO}$ is along either [110] or [1$\bar{1}$0], and $\vec{s}_{Fe}$ is always perpendicular to $\overleftrightarrow{s}_{CoO}$ due to the strong spin-flop coupling [33,35]. While applying H along [110], due to the Zeeman energy of the Fe layer, CoO domains with $\overleftrightarrow{s}_{CoO} \| [1\bar{1}0]$ have lower energy than those with $\overleftrightarrow{s}_{CoO} \| [110]$, thus H can drive the expansion of the CoO domain with $\overleftrightarrow{s}_{CoO} \perp H$. The DWs can be pinned by the local defects, and certain thermal excitation is required for the depinning of the AFM DWs, which can explain the faster AFM domain switching at higher temperature. As shown by the schematic drawing in Figs. 4(a) and 4(b), while only a dc field is applied, all the FM and AFM spins in domains and DWs are staying at the local minimum energy state, and are orthogonally coupled. However, if the field is reversed, $\vec{s}_{Fe}$ on top of the CoO AFM domains with $\overleftrightarrow{s}_{CoO} \| [1\bar{1}0]$ will reverse its direction, then $\vec{s}_{Fe}$ inside the DWs are rotated accordingly, as shown in Figs. 4(c) and 4(d). During the field switching process, $\vec{s}_{Fe}$ inside the DWs are not perpendicular to $\overleftrightarrow{s}_{CoO}$, thus $\overleftrightarrow{s}_{CoO}$ will experience a large transient torque due to the exchange coupling with $\vec{s}_{Fe}$. Such exchange torques can drive the AFM DW to overcome the local pinning, leading to expansion of the AFM domain. Our simulation proves that the FM spins can fully reverse within the nanosecond time scale, and it is expected that the faster switching of FM spins by stronger field will result in the stronger exchange torques inside the AFM domain walls.
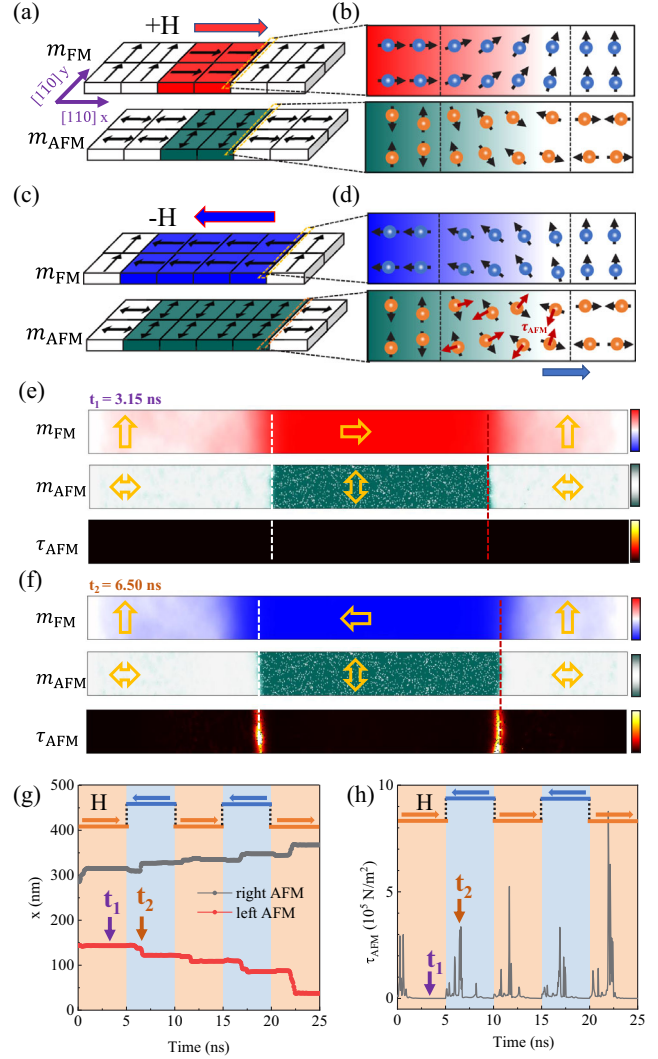
FIG. 4. Schematic illustrations of FM and AFM spins (a) before and (c) right after the field switching, with the enlarged spin structures shown in (b) and (d). Snapshots of spin dynamic simulations (e) at the stable state and (f) at the intermediate state right after the field switching, showing the strong torque inside the AFM domain walls. (g) The time-dependent positions of two AFM domain walls. (h) The time-dependent averaged torque acting on the AFM spins. The blue and orange regions in (g) and (h) mark the timespans of opposite fields.

In order to verify the scenario of the exchange torques inside the AFM DWs during the field reversal, we performed simulations on the dynamic switching of the ferromagnet-antiferromagnet bilayer utilizing the object oriented micromagnetic framework (OOMMF) package with a quasiatomistic approach [50]. The details can be found in the Supplemental Material [37]. As shown in Fig. 4(e), the simulation structure contains a FM-AFM bilayer with size of 425 nm × 25 nm. We first set $\overleftrightarrow{s}_{CoO}$ in the middle area of 100 nm along [1$\bar{1}$0] and the rest of the CoO spins along [110], then the system is relaxed to its equilibrium state. As expected, $\vec{s}_{Fe}$ is perpendicular to $\overleftrightarrow{s}_{CoO}$ at zero

field. The FM DWs are generally wider than the AFM DWs, which may be attributed to the large crystalline anisotropy of the AFM spins.

Then, we applied an ac field with $H_{ac} = 150$ Oe and $\Delta t = 5$ ns, and simulated the spin dynamics within 25 ns at 0 K. It should be noted that the spin state with three domains is unstable without any defects. Thus, in order to stabilize the AFM DWs under the magnetic field, we distributed nonmagnetic defects in the AFM layer as the wall pinning sites with a density of 8%, which provides the best match with our experimental results. In general, local defects are required to stabilize the AFM domains and generate local energy barriers for the motion of AFM DWs.

Our simulations show that, when the field is switched, the AFM DWs are moved and the middle domain is expanded. Figure 4(g) shows the extracted positions of left and right AFM DWs in the nanotrack as a function of time which exhibits a nearly steplike behavior. The domain wall position changes only after ~1 ns when the field is reversed, and keeps stable for the rest of the time. Because of the pinning effect, the speed of DW motion is usually on the order of ten meters per second. The torque on the AFM spins can also be calculated during the switching process. Figure 4(f) presents the distribution of FM spins, AFM spins, and the torque at $t = 6.5$ ns when the AFM DWs start to move, and the strong torque can be clearly observed at the positions of the AFM domain walls. Figure 4(h) shows the time-dependent torque of AFM spins inside the DWs, which always displays the peaks during AFM DW movements and should strongly depend on the sweeping slope of the ac field [37]. Our results also suggest that the pulse field with higher frequency could induce faster AFM domain switching, which is pivotal for designing fast storage devices based on the AFM domains.

In summary, we demonstrated the dynamic switching process of AFM spins in Fe/CoO bilayers can be directly imaged by the MOB effect under the applied fields. We found that alternating fields promote much faster switching process with smaller energy barrier for domain growth due to the strong exchange torque inside the AFM DWs, which was well proved by the spin dynamics simulations. Moreover, our study also provides a possible route to design novel information storage applications based on the ferromagnet-antiferromagnet bilayer, which can utilize the advantages of both FM and AFM spins. The information can be effectively installed into the AFM spins by the ac field, and is very stable in the ordinary environment with weak dc fields, but can be read out through the FM states due to the strong exchange coupling [37]. So, such spintronic devices based on the ferromagnet-antiferromagnet bilayer can reserve the advantages of both FM and AFM spins with high stability insensitive to the field, and overcome the shortcoming of a weak readout signal in the spintronic devices based on the single AFM layer.

---

*These authors contributed equally to this work.
†Corresponding author.
 zhouyan@cuhk.edu.cn
‡Corresponding author.
 wuyizheng@fudan.edu.cn

[1] T. Jungwirth, X. Marti, P. Wadley, and J. Wunderlich, Antiferromagnetic spintronics, Nat. Nanotechnol. **11**, 231 (2016).

[2] P. Wadley, B. Howells, J. Zelezny, C. Andrews, V. Hills, R. P. Campion, V. Novak, K. Olejnik, F. Maccherozzi, S. S. Dhesi, S. Y. Martin, T. Wagner, J. Wunderlich, F. Freimuth, Y. Mokrousov, J. Kunes, J. S. Chauhan, M. J. Grzybowski, A. W. Rushforth, K. W. Edmonds, B. L. Gallagher, and T. Jungwirth, Electrical switching of an antiferromagnet, Science **351**, 587 (2016).

[3] P. Wadley, S. Reimers, M. J. Grzybowski, C. Andrews, M. Wang, J. S. Chauhan, B. L. Gallagher, R. P. Campion, K. W. Edmonds, S. S. Dhesi, F. Maccherozzi, V. Novak, J. Wunderlich, and T. Jungwirth, Current polarity-dependent manipulation of antiferromagnetic domains, Nat. Nanotechnol. **13**, 362 (2018).

[4] S. Y. Bodnar, L. Smejkal, I. Turek, T. Jungwirth, O. Gomonay, J. Sinova, A. A. Sapozhnik, H. J. Elmers, M. Klaui, and M. Jourdan, Writing and reading antiferromagnetic Mn_2Au by Néel spin-orbit torques and large anisotropic magnetoresistance, Nat. Commun. **9**, 348 (2018).

[5] T. Moriyama, K. Oda, T. Ohkochi, M. Kimata, and T. Ono, Spin torque control of antiferromagnetic moments in NiO, Sci. Rep. **8**, 14167 (2018).

[6] X. Z. Chen, R. Zarzuela, J. Zhang, C. Song, X. F. Zhou, G. Y. Shi, F. Li, H. A. Zhou, W. J. Jiang, F. Pan, and Y. Tserkovnyak, Antidamping-Torque-Induced Switching in Biaxial Antiferromagnetic Insulators, Phys. Rev. Lett. **120**, 207204 (2018).

[7] L. Baldrati, O. Gomonay, A. Ross, M. Filianina, R. Lebrun, R. Ramos, C. Leveille, F. Fuhrmann, T. R. Forrest, F. Maccherozzi, S. Valencia, F. Kronast, E. Saitoh, J. Sinova, and M. Kläui, Mechanism of Néel Order Switching in Antiferromagnetic Thin Films Revealed by Magnetotransport and Direct Imaging, Phys. Rev. Lett. **123**, 177201 (2019).

[8] V. Baltz, A. Manchon, M. Tsoi, T. Moriyama, T. Ono, and Y. Tserkovnyak, Antiferromagnetic spintronics, Rev. Mod. Phys. **90**, 015005 (2018).

[9] A. S. Núñez, R. A. Duine, P. Haney, and A. H. MacDonald, Theory of spin torques and giant magnetoresistance in antiferromagnetic metals, Phys. Rev. B **73**, 214426 (2006).

[10] H. V. Gomonay and V. M. Loktev, Spin transfer and current-induced switching in antiferromagnets, Phys. Rev. B **81**, 144427 (2010).

[11] V. Bonbien, F. Zhuo, A. Salimath, O. Ly, A. Abbout, and A. Manchon, Topological aspects of antiferromagnets, J. Phys. D **55**, 103002 (2022).

[12] S. A. Siddiqui, J. Sklenar, K. Kang, M. J. Gilbert, A. Schleife, N. Mason, and A. Hoffmann, Metallic antiferromagnets, J. Appl. Phys. **128**, 040904 (2020).

[13] J. Železný, P. Wadley, K. Olejník, A. Hoffmann, and H. Ohno, Spin transport and spin torque in antiferromagnetic devices, Nat. Phys. **14**, 220 (2018).

[14] P. Němec, M. Fiebig, T. Kampfrath, and A. V. Kimel, Antiferromagnetic opto-spintronics, Nat. Phys. **14**, 229 (2018).

[15] X. Marti, I. Fina, C. Frontera, J. Liu, P. Wadley, Q. He, R. J. Paull, J. D. Clarkson, J. Kudrnovsky, I. Turek, J. Kunes, D. Yi, J. H. Chu, C. T. Nelson, L. You, E. Arenholz, S. Salahuddin, J. Fontcuberta, T. Jungwirth, and R. Ramesh, Room-temperature antiferromagnetic memory resistor, Nat. Mater. **13**, 367 (2014).

[16] D. Kriegner, K. Vyborny, K. Olejnik, H. Reichlova, V. Novak, X. Marti, J. Gazquez, V. Saidl, P. Nemec, V. V. Volobuev, G. Springholz, V. Holy, and T. Jungwirth, Multiple-stable anisotropic magnetoresistance memory in antiferromagnetic MnTe, Nat. Commun. **7**, 11623 (2016).

[17] K. Olejnik, V. Schuler, X. Marti, V. Novak, Z. Kaspar, P. Wadley, R. P. Campion, K. W. Edmonds, B. L. Gallagher, J. Garces, M. Baumgartner, P. Gambardella, and T. Jungwirth, Antiferromagnetic CuMnAs multi-level memory cell with microelectronic compatibility, Nat. Commun. **8**, 15434 (2017).

[18] S.-W. Cheong, M. Fiebig, W. Wu, L. Chapon, and V. Kiryukhin, Seeing is believing: Visualization of antiferromagnetic domains, npj Quantum Mater. **5**, 3 (2020).

[19] J. Stöhr, A. Scholl, T. J. Regan, S. Anders, J. Lüning, M. R. Scheinfein, H. A. Padmore, and R. L. White, Images of the Antiferromagnetic Structure of a NiO(100) Surface by Means of X-Ray Magnetic Linear Dichroism Spectromicroscopy, Phys. Rev. Lett. **83**, 1862 (1999).

[20] M. Bode, E. Y. Vedmedenko, K. von Bergmann, A. Kubetzka, P. Ferriani, S. Heinze, and R. Wiesendanger, Atomic spin structure of antiferromagnetic domain walls, Nat. Mater. **5**, 477 (2006).

[21] U. Kaiser, A. Schwarz, and R. Wiesendanger, Magnetic exchange force microscopy with atomic resolution, Nature (London) **446**, 522 (2007).

[22] I. Gross, W. Akhtar, V. Garcia, L. J. Martínez, S. Chouaieb, K. Garcia, C. Carrétéro, A. Barthélémy, P. Appel, P. Maletinsky, J. V. Kim, J. Y. Chauleau, N. Jaouen, M. Viret, M. Bibes, S. Fusil, and V. Jacques, Real-space imaging of non-collinear antiferromagnetic order with a single-spin magnetometer, Nature (London) **549**, 252 (2017).

[23] J. Y. Chauleau, E. Haltz, C. Carretero, S. Fusil, and M. Viret, Multi-stimuli manipulation of antiferromagnetic domains assessed by second-harmonic imaging, Nat. Mater. **16**, 803 (2017).

[24] I. Gray, T. Moriyama, N. Sivadas, G. M. Stiehl, J. T. Heron, R. Need, B. J. Kirby, D. H. Low, K. C. Nowack, D. G. Schlom, D. C. Ralph, T. Ono, and G. D. Fuchs, Spin Seebeck Imaging of Spin-Torque Switching in Antiferromagnetic Pt/NiO Heterostructures, Phys. Rev. X **9**, 041016 (2019).

[25] J. Xu, C. Zhou, M. Jia, D. Shi, C. Liu, H. Chen, G. Chen, G. Zhang, Y. Liang, J. Li, W. Zhang, and Y. Wu, Imaging antiferromagnetic domains in nickel oxide thin films by optical birefringence effect, Phys. Rev. B **100**, 134413 (2019).

[26] J. Xu, H. Chen, C. Zhou, D. Shi, G. Chen, and Y. Wu, Optical imaging of antiferromagnetic domains in ultrathin CoO(001) films, New J. Phys. **22**, 083033 (2020).

[27] F. Schreiber, L. Baldrati, C. Schmitt, R. Ramos, E. Saitoh, R. Lebrun, and M. Kläui, Concurrent magneto-optical imaging and magneto-transport readout of electrical switching of insulating antiferromagnetic thin films, Appl. Phys. Lett. **117**, 082401 (2020).

[28] C. C. Chiang, S. Y. Huang, D. Qu, P. H. Wu, and C. L. Chien, Absence of Evidence of Electrical Switching of the Antiferromagnetic Néel Vector, Phys. Rev. Lett. **123**, 227203 (2019).

[29] P. Zhang, J. Finley, T. Safi, and L. Liu, Quantitative Study on Current-Induced Effect in an Antiferromagnet Insulator/ Pt Bilayer Film, Phys. Rev. Lett. **123**, 247206 (2019).

[30] Y. Cheng, S. Yu, M. Zhu, J. Hwang, and F. Yang, Electrical Switching of Tristate Antiferromagnetic Néel Order in α-Fe$_2$O$_3$ Epitaxial Films, Phys. Rev. Lett. **124**, 027202 (2020).

[31] S. P. Bommanaboyena, D. Backes, L. S. I. Veiga, S. S. Dhesi, Y. R. Niu, B. Sarpi, T. Denneulin, A. Kovács, T. Mashoff, O. Gomonay, J. Sinova, K. Everschor-Sitte, D. Schönke, R. M. Reeve, M. Kläui, H. J. Elmers, and M. Jourdan, Readout of an antiferromagnetic spintronics system by strong exchange coupling of Mn$_2$Au and Permalloy, Nat. Commun. **12**, 6539 (2021).

[32] A. Scholl, M. Liberati, E. Arenholz, H. Ohldag, and J. Stohr, Creation of an Antiferromagnetic Exchange Spring, Phys. Rev. Lett. **92**, 247201 (2004).

[33] Q. Li, G. Chen, T. P. Ma, J. Zhu, A. T. N'Diaye, L. Sun, T. Gu, Y. Huo, J. H. Liang, R. W. Li, C. Won, H. F. Ding, Z. Q. Qiu, and Y. Z. Wu, Activation of antiferromagnetic domain switching in exchange-coupled Fe/CoO/MgO(001) systems, Phys. Rev. B **91**, 134428 (2015).

[34] Q. Li, T. Gu, J. Zhu, Z. Ding, J. X. Li, J. H. Liang, Y. M. Luo, Z. Hu, C. Y. Hua, H. J. Lin, T. W. Pi, C. Won, and Y. Z. Wu, Multiple in-plane spin reorientation transitions in Fe/CoO bilayers grown on vicinal MgO(001), Phys. Rev. B **91**, 104424 (2015).

[35] Q. Li, T. P. Ma, M. Yang, L. Sun, S. Y. Huang, R. W. Li, C. Won, Z. Q. Qiu, and Y. Z. Wu, Field dependence of antiferromagnetic domain switching in epitaxial Fe/CoO/MgO(001) systems, Phys. Rev. B **96**, 024420 (2017).

[36] Y. Yang, J. Liang, Q. Li, G. Chen, C. Zhou, J. Xu, L. Sun, M. Yang, A. T. N'Diaye, Z. Q. Qiu, and Y. Wu, Antiferromagnetic domain switching modulated by an ultrathin Co interlayer in the Fe/Co/CoO/MgO(001) system, Phys. Rev. B **102**, 024434 (2020).

[37] See Supplemental Material at http://link.aps.org/supplemental/10.1103/PhysRevLett.128.137201 for the growth quality of samples, detailed description of the data analysis methods mentioned in the text, and the detailed method on spin dynamics simulations, which includes Refs. [25,27,29,30,33,35,38–46].

[38] I. V. Soldatov and R. Schäfer, Advances in quantitative Kerr microscopy, Phys. Rev. B **95**, 014426 (2017).

[39] I. V. Soldatov and R. Schafer, Selective sensitivity in Kerr microscopy, Rev. Sci. Instrum. **88**, 073701 (2017).

[40] J. Miguel, R. Abrudan, M. Bernien, M. Piantek, C. Tieg, J. Kirschner, and W. Kuch, Magnetic domain coupling study in single-crystalline Fe/CoO bilayers, J. Phys. Condens. Matter **21**, 185004 (2009).

[41] W. N. Cao, J. Li, G. Chen, J. Zhu, C. R. Hu, and Y. Z. Wu, Temperature-dependent magnetic anisotropies in epitaxial Fe/CoO/MgO(001) system studied by the planar Hall effect, Appl. Phys. Lett. **98**, 262506 (2011).

[42] W. Wernsdorfer, E. B. Orozco, K. Hasselbach, A. Benoit, B. Barbara, N. Demoncy, A. Loiseau, H. Pascard, and D. Mailly, Experimental Evidence of the Néel-Brown Model of Magnetization Reversal, Phys. Rev. Lett. **78**, 1791 (1997).

[43] J. Barker and O. A. Tretiakov, Static and Dynamical Properties of Antiferromagnetic Skyrmions in the Presence of Applied Current and Temperature, Phys. Rev. Lett. **116**, 147203 (2016).

[44] G. Fischer, M. Däne, A. Ernst, P. Bruno, M. Lüders, Z. Szotek, W. Temmerman, and W. Hergert, Exchange coupling in transition metal monoxides: Electronic structure calculations, Phys. Rev. B **80**, 014408 (2009).

[45] W. Eerenstein, T. T. Palstra, S. S. Saxena, and T. Hibma, Spin-polarized transport across sharp antiferromagnetic boundaries, Phys. Rev. Lett. **88**, 247204 (2002).

[46] R. G. S. Sofin, H.-C. Wu, and I. V. Shvets, Anomalous magnetization reversal due to proximity effect of antiphase boundaries, Phys. Rev. B **84**, 212403 (2011).

[47] H. Xi, S. Franzen, S. Mao, and R. M. White, Exchange bias relaxation in reverse magnetic fields, Phys. Rev. B **75**, 014434 (2007).

[48] A. Hoffmann, Symmetry Driven Irreversibilities at Ferromagnetic-Antiferromagnetic Interfaces, Phys. Rev. Lett. **93**, 097203 (2004).

[49] H. Xi, K.-Z. Gao, J. Ouyang, Y. Shi, and Y. Yang, Slow magnetization relaxation and reversal in magnetic thin films, J. Phys. Condens. Matter **20**, 295220 (2008).

[50] M. J. Donahue and D. G. Porter, *OOMMF User's Guide, Version 1.0* (National Institute of Standard and Technology, Gaithersburg, MD, 1999), Interagency Report NISTIR.